Influence of the Benzoquinone Sorption on the Structure and Electrochemical Performance of the MIL-53(Fe) Hybrid Porous Material in a Lithium-Ion Battery

G. de Combarieu,[†] M. Morcrette,[†] F. Millange,[‡] N. Guillou,[‡] J. Cabana,[§] C. P. Grey,[§] I. Margiolaki,[⊥] G. Férey,[‡] and J.-M. Tarascon*,[†]

LRCS, UMR CNRS 6007, Université de Picardie Jules Verne, 33 Rue Saint Leu, 80039 Amiens, France, Institut Lavoisier de Versailles, UMR CNRS 8180, Université de Versailles St-Quentin-en-Yvelines, 45 avenue des Etats Unis, 78035 Versailles, France, Department of Chemistry, State University of New York at Stony Brook, Stony Brook, New York, 11794-3400, and ID31, Materials Science Group, European Synchrotron Radiation Facility, BP 220, 38043 Grenoble, France

Received December 1, 2008. Revised Manuscript Received January 29, 2009

Among the metal-organic frameworks (MOFs), **MIL-53(Fe)** or $Fe^{III}(OH)_{0.8}F_{0.2}[O_2C-C_6H_4-CO_2]$ was the first ever reported member to reversibly insert Li^+ electrochemically. A variety of electroactive sorbents has been investigated in an attempt to increase its electrochemical capacity vs Li^+/Li^0. Here, we describe the synthesis and characterization of a new composite hybrid material involving **MIL-53(Fe)** as the host for the guest electroactive 1,4-benzoquinone molecule in a 1:1 molar ratio, using complementary high-resolution X-ray diffraction (XRD), differential scanning calorimetry (DSC), and magic angle spinning nuclear magnetic resonance (MAS NMR) measurements. Its room-temperature structure has been solved and shows that the quinone molecules are located within the channels nearly parallel to each other, and to the benzene rings of the skeleton, in order to maximize $\pi-\pi$ interactions. When heated in a sealed container, a flip-flop reorganization of the quinone molecules occurred above 140 °C, whereas in an open environment, desorption of the quinone was shown near 120 °C giving rise to a new phase having solely 0.5 quinone molecules/**MIL-53(Fe)** formula unit. Enhancement of the electrochemical performances, due to the redox properties of the quinone molecules, was observed during the first 2 cycles. An exchange between both the quinone and the electrolyte molecules is proposed to account for the capacity decay in subsequent cycles.

1. Introduction

The field of porous materials, which for many decades has largely focused on inorganic solids with open-framework structures (such as zeolites and their analogues), has been recently revitalized by the discovery of metal-organic frameworks (MOFs).[1−3] These solids combine inorganic metal clusters or coordination centers with organic linkers to yield a diversity of three-dimensional structures with porosities that span those exhibited by the well-known microporous zeolites and the mesoporous silicas. One of the most important features of the chemistry of the metal-organic framework materials is their interaction with small molecules for applications in gas separation and storage, and this is where they are likely to offer significant benefits over traditional zeolite materials.[4] For example, MOFs have been the subject of intense investigation regarding reversible hydrogen storage where their organic structural subunits might offer high concentrations of some significant binding sites.[5−8] MOFs have also shown very favorable CO_2 sorption properties,[9−11] and some of the materials present some of the highest surface areas seen for crystalline inorganic solids.[12−14] Other applications have also recently emerged, for example, in the areas of drug delivery[15] and catalysis.[16] In very recent work, we have tested Fe^{3+}-MOFs to determine

* Corresponding author. E-mail: jean-marie.tarascon@u-picardie.fr.
[†] Université de Picardie Jules Verne.
[‡] Université de Versailles St-Quentin-en-Yvelines.
[§] State University of New York at Stony Brook.
[⊥] European Synchrotron Radiation Facility.

(1) Férey, G. *Chem. Soc. Rev.* **2008**, *37*, 191.
(2) Yaghi, O. M.; O'Keeffe, M.; Ockwig, N. W.; Chae, H. K.; Eddaoudi, M.; Kim, J. *Nature* **2003**, *423*, 705.
(3) Kitagawa, S.; Kitaura, R.; Noro, S. *Angew. Chem., Int. Ed.* **2004**, *43*, 2334.
(4) Mueller, U.; Schubert, M.; Teich, F.; Puetter, H.; Schierle-Arndt, K.; Pastre, J. *J. Mater. Chem.* **2006**, *16*, 626.
(5) Latroche, M.; Surblé, S.; Serre, C.; Mellot-Draznieks, C.; Llewellyn, P. L.; Lee, J. H.; Chang, J. S.; Jhung, S. H.; Férey, G. *Angew. Chem., Int. Ed.* **2006**, *45*, 8227.
(6) Lin, X.; Jia, J. H.; Hubberstey, P.; Schroder, M.; Champness, N. R. *CrystEngComm.* **2007**, *9*, 438.
(7) Zhao, X. B.; Xiao, B.; Fletcher, A. J.; Thomas, K. M.; Bradshaw, D.; Rosseinsky, M. J. *Science* **2004**, *306*, 1012.
(8) Rosi, N. L.; Eckert, J.; Eddaoudi, M.; Vodak, D. T.; Kim, J.; O'Keeffe, M.; Yaghi, O. M. *Science* **2003**, *300*, 1127.
(9) Llewellyn, P. L.; Bourrelly, S.; Serre, C.; Vimont, A.; Daturi, M.; Hamon, L.; De Weireld, G.; Chang, J. S.; Hong, D. Y.; Hwang, Y. K.; Jhung, S. H.; Férey, G. *Langmuir* **2008**, *24*, 7245.
(10) Bourrelly, S.; Llewellyn, P. L.; Serre, C.; Millange, F.; Loiseau, T.; Férey, G. *J. Am. Chem. Soc.* **2005**, *127*, 13519.
(11) Millward, A. R.; Yaghi, O. M. *J. Am. Chem. Soc.* **2005**, *127*, 17998.
(12) Chae, H. K.; Siberio-Perez, D. Y.; Kim, J.; Go, Y.; Eddaoudi, M.; Matzger, A. J.; O'Keeffe, M.; Yaghi, O. M. *Nature* **2004**, *427*, 523.
(13) Férey, G.; Serre, C.; Mellot-Draznieks, C.; Millange, F.; Surblé, S.; Dutour, J.; Margiolaki, I. *Angew. Chem., Int. Ed.* **2004**, *43*, 6296.
(14) Férey, G.; Mellot-Draznieks, C.; Serre, C.; Millange, F.; Dutour, J.; Surblé, S.; Margiolaki, I. *Science* **2005**, *309*, 2040.
(15) Horcajada, P.; Serre, C.; Maurin, G.; Ramsahye, N. A.; Balas, F.; Vallet-Regi, M.; Sebban, M.; Taulelle, F.; Ferey, G. *J. Am. Chem. Soc.* **2008**, *130*, 6774.

10.1021/cm8032324 CCC: $40.75
Published on Web 04/02/2009

whether they represent possible positive electrode materials in lithium cells and whether it is possible to take advantage of the large pores in the structure as empty spaces to host lithium cations.[17] This electrochemical reactivity is due to the possibility of reducing Fe^{3+} to Fe^{2+} along with the simultaneous insertion of Li^+ in the structure. Up to 0.6 lithium cation per iron Fe^{3+} can be inserted into the MIL-53(Fe) structure at a *C*/40 rate without any structural alteration to the framework. This was the first demonstration of the use of a MOF structure as a positive intercalation compound in a lithium battery. Despite these good properties, neither the volumetric (mA h cm^{-3}) nor the gravimetric (mA h g^{-1}) electrochemical capacities were very high, because of both the low density of the material and the limited number of inserted Li^+. Moreover, we saw limited cyclability at high energy density because of the poor electronic conductivity of the structure. This poor electronic conductivity was rationalized in terms of interactions between Fe^{3+} and Fe^{2+} sites, which do not allow any electronic delocalization.[18] To push back these two limits, we decided to increase the capacity through the adsorption of an electroactive molecule, i.e., 1,4-benzoquinone, which can theoretically accept two electrons per molecule but can also play a role as a redox mediator enhancing the electronic transfer in the **MIL-53(Fe)** structure.

In this paper, we first characterize the new composite structure formed following sorption of quinone molecules in the pores of the pristine **MIL-53(Fe)**. We then evaluate its electrochemical properties in a classical lithium cell. A mechanism to take into account the electrochemical properties is put forward on the basis of the information obtained from in situ X-ray diffraction and NMR spectroscopy.

2. Experimental Section

2.1. Synthesis. MIL-53(Fe)_H_2O used in this study has been synthesized as reported in previous studies.[19,20] **MIL-53(Fe)_H_2O** was isolated as a phase-pure pale orange crystalline powder under solvothermal conditions from an equimolar amount of iron(III) chloride hydrate $FeCl_3 \cdot xH_2O$ (Aldrich, 97%), 1,4-benzenedicarboxylic acid HO_2C-(C_6H_4)-CO_2H (Alfa 97%), hydrofluoric acid HF (Prolabo, 40%) in *N*,*N*′-dimethylformamide (DMF, Aldrich 99%). Reactants were stirred for a few minutes prior to introducing the resulting suspension into a Teflon-lined steel autoclave, and the temperature was set at 423 K for 1 day. The light orange **MIL-53(Fe)_H_2O** powder was finally obtained after dispersion of the solvothermally synthesized powder into a large amount of water for 2 h. This solid was then dehydrated under a primary vacuum at 373 K (Büchi oven, 1 h) to remove structural water molecules adsorbed in the channels and obtain the anhydrous form at room temperature denoted **MIL-53(Fe)_vac**. The 1,4-benzoquinone molecules were sorbed by simply hand-milling in a mortar a mixture of *y* mole of 1,4-benzoquinone and 1 mol of **MIL-53(Fe)_vac** for a few minutes under an argon atmosphere. The mixture was then allowed to equilibrate for 2 days at room temperature in the (Ar) glovebox, and the new solid obtained is noted hereafter **MIL-53(Fe)_(quinone)$_y$**.

2.2. Powder X-ray Diffraction. A number of powder X-ray diffraction methods were used to characterize the solid. The X-ray powder diffraction patterns of the **MIL-53(Fe)_(quinone)$_y$** solids were first recorded on a Bruker D8 Advance diffractometer ($\theta-2\theta$ mode, Co K_α radiation $\lambda = 1.7903$ Å, and a linear position-sensitive detector). To carry out the in situ X-ray diffraction experiments, a modified Swagelok-type cell[21] was mounted horizontally and monitored by a MacPile (Biologic SA, Claix, France) system in a galvanostatic mode at a *C*/10 regime, between 1.8 and 3.5 V vs Li^+/Li^0, to collect the X-ray data.

Additionally, for the newly identified phases, high-resolution powder X-ray diffraction data were collected on the station ID31 at the ESRF from powdered samples contained in 1 mm diameter quartz capillaries. The beam line receives X-rays from the synchrotron source (which operates with an average energy of about 6 GeV) from an undulator device. The incident X-ray wavelength was about 0.8 Å using an incident beam size of 2.0 mm (horizontal) × 1.0 mm (vertical). The sample was rapidly spun during data collection to ensure good powder averaging. Extractions of the peak positions, pattern indexing and Rietveld refinements were carried out with the TOPAS program.[22] Direct methods calculations were performed with the EXPO package[23,24] and the structural model was completed by using simulated annealing with TOPAS. In the process of Rietveld refinement, the terephthalate ions as well as quinone molecules were treated as rigid bodies.

Temperature-dependent X-ray powder diffraction measurements were performed using Siemens D5000 diffractometer ($\theta-\theta$ mode, Co K_α radiation and a PSD) equipped with an Anton Paar HTK1200 high-temperature device under a N_2 atmosphere.

2.3. Thermal Analysis. The thermal characterization of **MIL-53(Fe)_(quinone)$_y$** was performed using differential scanning calorimetry (DSC) with a Netzsch DSC 204F1 "Phoenix" apparatus, from room temperature to 350 °C under flowing Ar (25 mL/min) at a 5 °C/min heating rate. Additionally, thermogravimetric analyses were performed on a Netzsch STA 449 "Jupiter" apparatus, from room temperature to 500 °C under flowing Ar (25 mL/min) at a 5 °C/min heating rate.

2.4. NMR Experiments. ^7Li and ^{13}C MAS NMR experiments were performed with a double-resonance 1.8 mm probe, built by A. Samoson and co-workers (KBFI, Tallinn, Estonia), on a CMX-200 spectrometer using a magnetic field of 4.7 T. The spectra were collected at an operating frequency of 77.71 and 50.28 MHz, respectively; a spinning frequency of 38 kHz and a rotor-synchronized spin−echo sequence (90°-τ−180°-τ-acq) were used. The $\pi/2$ pulse widths were 2.7 and 3.0 μs for the ^7Li and ^{13}C measurements and delay times of 0.2 s were used in all cases, respectively. The ^7Li spectra were referenced to a 1 M LiCl solution, at 0 ppm. In the case of the ^{13}C study, a ^{13}C-enriched glycine was used as a secondary standard to reference to TMS. The resonance due to the carboxylic group in this compound was set at 175 ppm. All the samples recovered from discharged cells were packed into the NMR rotors in an Ar-filled glovebox.

(16) Hwang, Y. K.; Hong, D. Y.; Chang, J. S.; Jhung, S. H.; Seo, Y. K.; Kim, J.; Vimont, A.; Daturi, M.; Serre, C.; Férey, G. *Angew. Chem., Int. Ed.* **2008**, *47*, 4144.
(17) Férey, G.; Millange, F.; Morcrette, M.; Serre, C.; Doublet, M. L.; Grenèche, J. M.; Tarascon, J. M. *Angew. Chem., Int. Ed.* **2007**, *46*, 3259.
(18) Combelles, C.; Doublet, M. L. *Ionics* **2008**, *14*, 279.
(19) Millange, F.; Serre, C.; Guillou, N.; Férey, G.; Walton, R. I. *Angew. Chem., Int. Ed.* **2008**, *47*, 4100.
(20) Millange, F.; Guillou, N.; Walton, R. I.; Grenèche, J. M.; Margiolaki, I.; Férey, G. *Chem. Commun.* **2008**, 4732.
(21) Morcrette, M.; Chabre, Y.; Vaughan, G.; Amatucci, G.; Leriche, J. B.; Patoux, S.; Masquelier, C.; Tarascon, J. M. *Electrochim. Acta* **2002**, *47*, 3137.
(22) *TOPAS V3.0: General Profile and Structure Analysis Software for Powder Diffraction Data*; Bruker AXS Ltd: Madison, WI, 2004.
(23) Altomare, A.; Caliandro, R.; Camalli, M.; Cuocci, C.; Giacovazzo, C.; Moliterni, A. G. G.; Rizzi, R. *J. Appl. Crystallogr.* **2004**, *37*, 1025.
(24) Altomare, A.; Cuocci, C.; da Silva, I.; Giacovazzo, C.; Moliterni, A. G. G.; Rizzi, R. *Powder Diffr.* **2005**, *20*, 327.

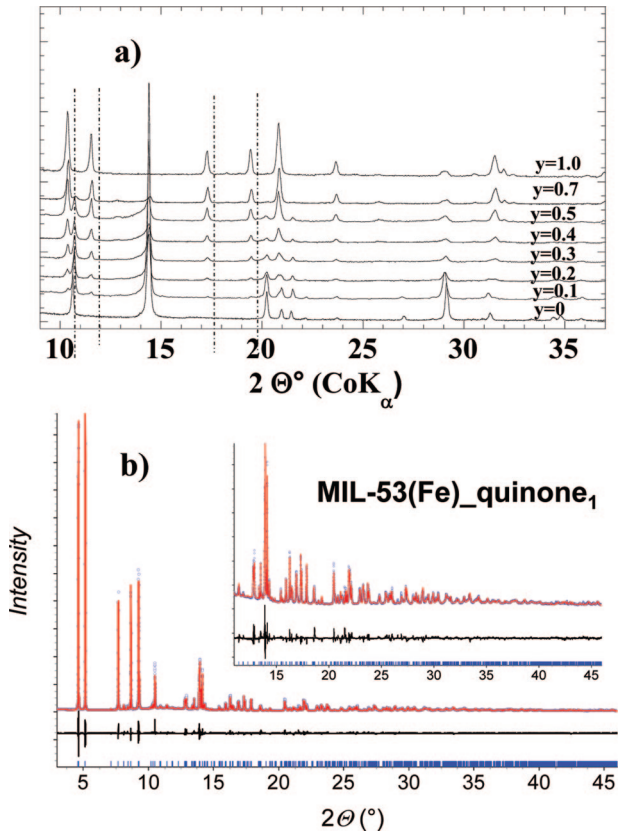

Figure 1. (a) X-Ray diffraction of **MIL-53(Fe)_quinone$_y$** with various equivalents of 1,4-benzoquinone (y) 0, 0.1, 0.2, 0.3, 0.4, 0.5, 0.7, and 1.0. (b) Rietveld refinement for **MIL-53(Fe)_quinone$_1$** from XRD data collected on ID31 at the ESRF.

2.5. Electrochemistry. Electrochemical tests were performed in standard Swagelok cells with lithium foil as the negative electrode and a **MIL-53(Fe)_quinone$_y$**/carbon composite as the positive electrode. A Whatman GF/D borosilicate glass fiber sheet saturated with a 1 M $LiPF_6$ electrolyte solution in 1:1 (w/w) of dimethyl carbonate (DMC)/ethylene carbonate (EC) constitutes the separator membrane (commercial LP30 electrolyte). The active material powder together with 20% (mass %) Super P carbon (SP, MMM Carbon, Belgium) were hand-milled in an agate mortar. A VMP automatic cycling/data recording system (Biologic SA, Claix, France) operating in potentiostatic mode (with galvanostatic acceleration) at a *C*/10 regime was used to record the electrochemical data. The cells were cycled between 1.8 and 3.5 V vs Li^+/Li^0.

3. Results and Discussion

3.1. Structure−Composition Relation. To prepare the quinone-loaded samples, we first dehydrated **MIL-53(Fe)_H_2O** by heating it at 373 K under a vacuum to get **MIL-53(Fe)_vac**. This procedure results in a decrease in the pore volume. Starting from **MIL-53(Fe)_vac**, several materials **MIL-53(Fe)_quinone$_y$** with ($0 < y < 1$) were prepared (see Figure 1a). As soon as the 1,4-benzoquinone molecule is introduced, the peaks of **MIL-53(Fe)_vac** decrease and completely disappear for $y = 1$, leading to the new phase **MIL-53(Fe)_quinone$_1$** (Figure 1a). The unit cell and space group were found unambiguously from synchrotron X-ray powder diffraction with a satisfactory figure of merit ($M_{20} = 25$).[25] **MIL-53(Fe)_quinone$_1$** crystallizes at room temperature in the $P2_1/c$ space group [$a = 11.9140(2)$ Å, $b = 6.8775(2)$ Å, $c = 21.3414(3)$ Å, $\beta = 123.67(2)°$, and $V = 1455.33(4)Å^3$], The final Rietveld plot (Figure 1b) has satisfactory crystal structure model indicators ($R_B = 0.031$) and profile factors ($R_P = 0.070$ and $R_{WP} = 0.096$). In this compound, the Fe^{3+} cation is 6-fold coordinated in a distorted octahedral geometry and the octahedral M−O centers are linked by sharing *trans*-hydroxyl groups forming bent M−(OH/F)−M chains. Bond valence calculations[26,27] and infrared spectroscopy gave further evidence for the presence of this μ_2-hydroxyl group. The oxygen atoms of the BDC moieties occupy the equatorial positions of the $MO_4(OH/F)_2$ octahedra, whereas the OH/F groups occupy the shared positions between adjacent octahedra along the chain. The axial oxygen atom corners are shared by neighboring octahedra to form a zigzag $-OH/F-Fe^{3+}-OH/F-Fe^{3+}-$ backbone. The metal oxide chains in these compounds are parallel to each other and are cross-linked by the dianions to form a framework with an array of 1D diamond-shaped channels. Each channel is formed by four walls of benzyl units and four chains of corner-shared octahedra. At room temperature, **MIL-53(Fe)_quinone$_1$** contains guest molecules lying inside the channels that are nearly parallel to half of the four organic walls (Figure 2a). Double chains of quinone molecules are aligned along the metal oxide chains, with a shift of half of the *b* axis between organic moieties of two adjacent chains. In contrast to what it is observed with pyridine,[28] the quinone molecules are not hydrogen-bonded to the hydrophilic part of the octahedral chain but interact through $\pi-\pi$ interactions both (i) between equivalent neighboring quinone molecules of two adjacent chains and (ii) between quinone molecules and the benzyl units of the dicarboxylate linkers (Figure 2b).

3.2. Thermal Properties of MIL-53(Fe)_quinone$_1$. Figure 3a shows the thermogravimetric curve (TG) of **MIL-53(Fe)_quinone$_1$**. Two different mass losses were observed: one starting at 120 °C with a maximum at 140 °C and a second one starting at 160 °C with a maximum at 200 °C. Each of these two steps corresponds to the departure of half of a molecule of 1,4-benzoquinone (i.e., 15.5% of the mass of the pristine compound). Such a hypothesis was confirmed by XRD, as the compound cooled from 250 °C to room temperature under an inert atmosphere shows the powder pattern of **MIL-53(Fe)_vac**. Increasing the temperature to 450 °C was shown to result in a full decomposition of the material. The DSC study of **MIL-53(Fe)_quinone$_1$**was first performed in a sealed crucible to prevent any gaseous quinone molecules from departing. The DSC trace for **MIL-53(Fe)_quinone$_1$** exhibits two well-defined features located at 140 and 180 °C, both being reversible with decreasing the temperature (Figure 3a inset). These temperatures are in good agreement with those observed on the TGA curve, corresponding to the two-step departure of the quinone molecules. For the sake of comparison, we note that these

(25) De Wolff, P. M. *J. Appl. Crystallogr.* **1968**, *12*, 60.
(26) Okeeffe, M.; Brese, N. E. *Acta Crystallogr., Sect. B* **1992**, *48*, 152.
(27) Brese, N. E.; Okeeffe, M. *Acta Crystallogr., Sect. B* **1991**, *47*, 192.
(28) Whitfield, T. R.; Wang, X. Q.; Liu, L. M.; Jacobson, A. J. *Solid State Sci.* **2005**, *7*, 1096.

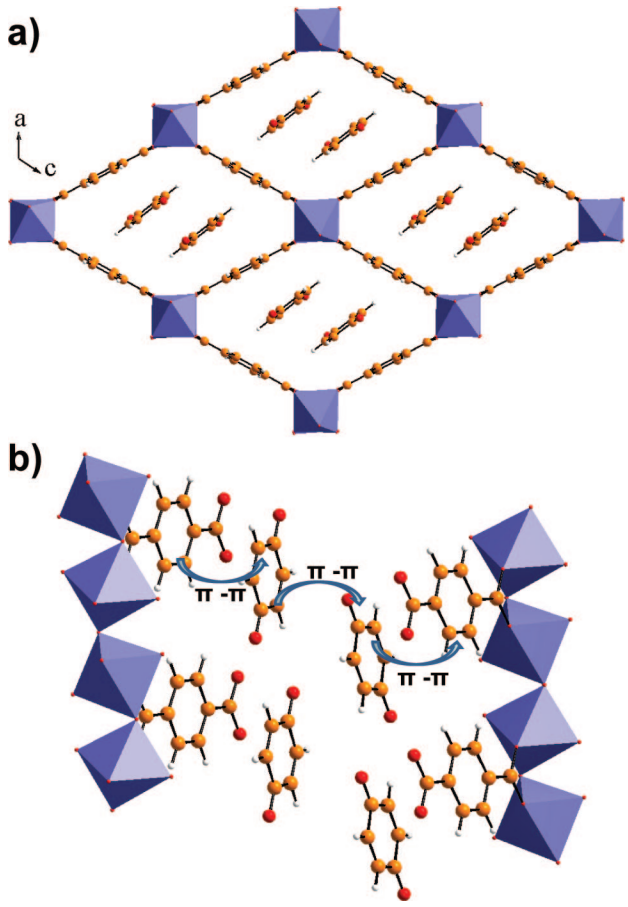

Figure 2. Drawing of the unit **MIL-53(Fe)_quinone$_1$** structure with, in (a) and (b), different views showing the global and detailed interactions between the host quinone molecules and the MOF linkers.

two peaks are not reversible when an open crucible is used instead of a sealed one. The change in the sublimation temperature between molecules (115 °C, see Figure 3a inset) to the two well-defined features (140 and 180 °C) for quinone in the MOF is illustrative of the weak interactions between both the quinone and the MOF-type structure and between the guests themselves inside the pores.

To get an insight into possible structural changes associated to the partial temperature-driven release of quinone from the MIL-53(Fe) structure, we performed in situ X-ray diffraction measurements between room temperature and 280 °C. Two experiments were conducted. In the first one (labeled open), the sample volume was constantly flushed with N_2 gas, whereas in the second one (labeled closed), the powder was placed in a sealed container having an autogenous N_2 pressure of 1 bar at room temperature. The evolution of the diffractograms for **MIL-53(Fe)_quinone$_1$** is reported in both panels a and b in Figure 4 for samples under open and closed N_2 atmospheres, respectively. For the sample heated in an open atmosphere, the **MIL-53(Fe)_quinone$_1$** mother phase progressively vanishes at the expense of a new phase associated with intense reflections located near 10.8, 12.3, and 24.9°(2θ). A single-phase is observed for a temperature reaching ∼120 °C (Figure 4a). Upon further increasing of the temperature, this new phase converts into a new intermediate phase at ∼160 °C that evolves rapidly into the **MIL-53(Fe)_ht** phase (ht for high temperature).[20] Surprisingly, for the sample heated in a closed atmosphere up to 160 °C,

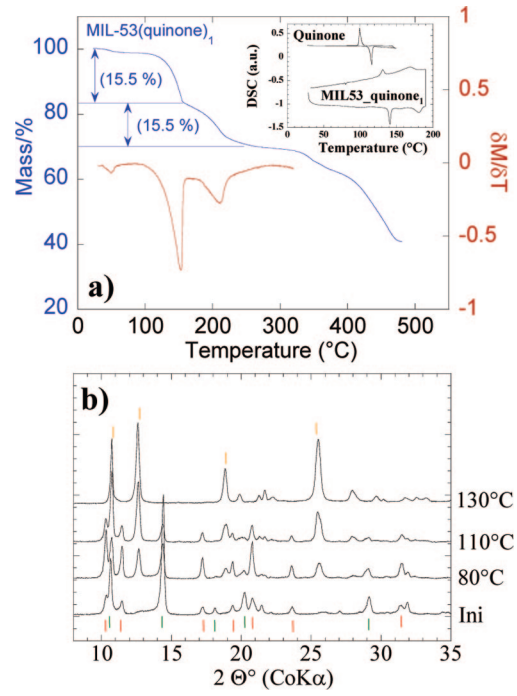

Figure 3. TGA experiment performed under an Ar flow from 25 °C up to 500 at 10 °C/min together with, as an inset, the DSC for the **MIL-53(Fe)_quinone$_1$** and pure quinone phase for comparison. Such measurements were done in sealed Al pans. Note the reversibility of the 140 and 180 °C transitions displayed by the **MIL-53(Fe)_quinone$_1$** sample. (b) XRD patterns obtained for samples of nominal composition **MIL-53(Fe)_quinone$_{0.5}$**, following heat treatment at various temperatures.

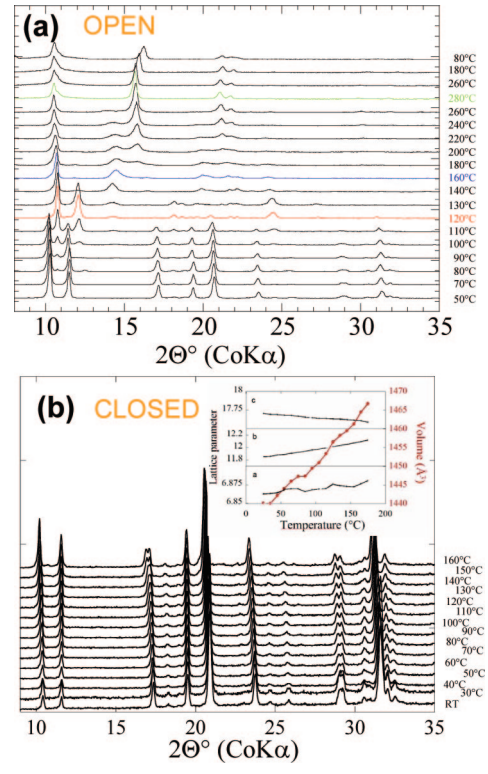

Figure 4. In situ temperature X-ray diffraction measurements for a MIL-53(Fe)_quinone$_1$ sample performed both under (a) open and (b) sealed Ar atmosphere. The data was collected on the way up and down, between room temperature and 160 and 260 °C in steps of 10 °C, respectively. Only the most representative XRDs are reported.

there is no clear evidence for a phase transformation, but a rather a pronounced continuous shift of the Bragg peaks is observed

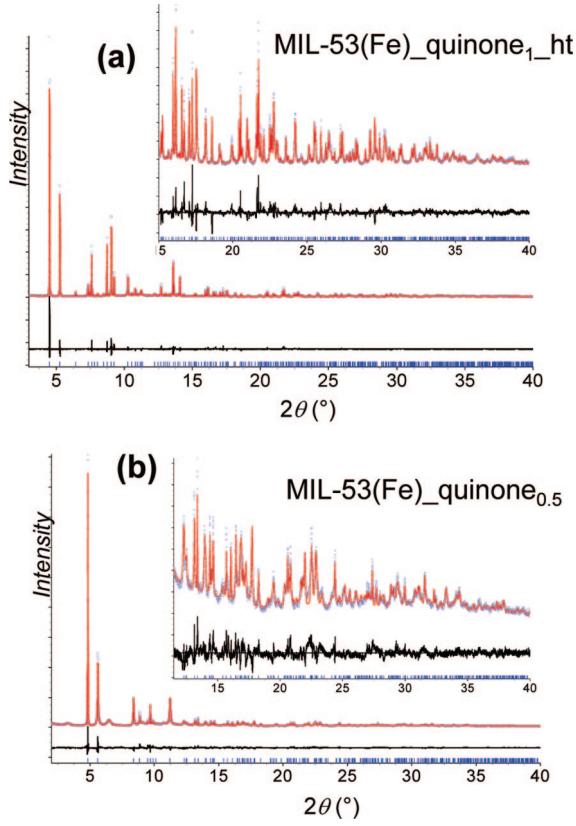

Figure 5. Rietveld refinements of the XRD powder patterns obtained for the **MIL-53(Fe)_quinone$_1$** phase, which was heated to 140 °C, in either (a) sealed or (b) open atmospheres. The data were collected on ID31 at the ESRF. Note that the quinone content for the sample run in open atmosphere is no longer 1 but 0.5.

(Figure 4b), which cannot be ascribed to temperature-driven volume expansion. A post TGA experiment has shown that the quinone content remained unchanged (i.e., 1 molecule per formula unit) for the sample heated at 160 °C. The apparent discrepancy between the results could come as a surprise, given that our DSC data in a sealed Al pan showed that the departure of the quinone occurred at 140 °C. This is simply rooted in a volume effect as the dead space above the XRD capillary is much smaller than in the DSC Al pan, hence altering the equilibrium for quinone desorption.

At this stage, high-resolution synchrotron XRD data were collected to obtain better insights into the structural changes of the temperature-driven **MIL-53(Fe)_quinone$_1$**. First, heating the **MIL-53(Fe)_quinone$_1$** phase in a sealed capillary at 140 °C led to the new phase labeled **MIL-53(Fe)_quinone$_1$_ht**. It crystallizes in an orthorhombic unit cell [a = 17.3814(3) Å, b = 6.8888(2) Å, c = 12.4796(2) Å, V = 1494.3(4) Å^3; SG: $Pn2_1a$, M_{20} = 254]. The final Rietveld plot (Figure 5a) is associated with a satisfactory crystal structure model indicator (R_B = 0.044) and profile factors (R_P = 0.073 and R_{WP} = 0.098). It is obvious under these conditions that the guest molecules cannot leave the pores, and only a reorganization of half of the quinone double chains is clearly observed. Within the same tunnel, the double chain is still nearly parallel to half of the four organic walls, whereas the double chain is tilted in order to be nearly parallel to the second half of the four organic walls in the nearest neighboring tunnels (Figure 6). This phenomenon can be described as a "flip flop effect". On the other hand,

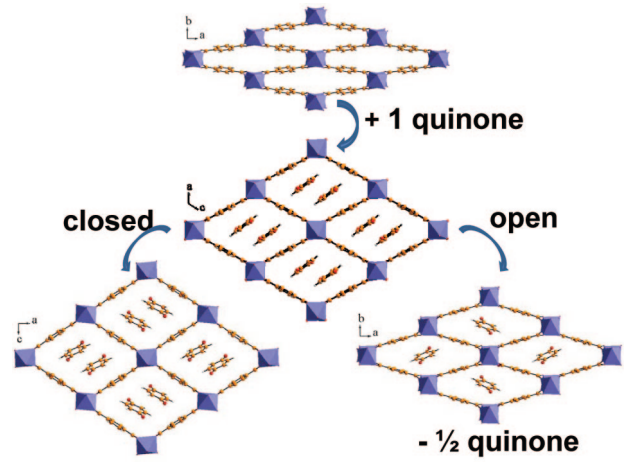

Figure 6. Recapturing the temperature-driven structural evolution of the **MIL-53(Fe)_quinone$_1$** phase as a function of the heating conditions, in closed or open environments.

under an open atmosphere, a different thermal behavior appears. A new phase has been isolated that crystallizes in a monoclinic unit cell [a = 19.767(1) Å, b = 9.0697(7) Å, c = 6.8753(3) Å, β = 106.814(5)° and V = 1179.9(1) Å^3; SG: Cc, M_{20} = 50]. The decrease in volume (~21%) is correlated to the departure of half of the quinone guest molecules from the pores leading to **MIL-53(Fe)_quinone$_{0.5}$**. The final Rietveld plot (Figure 5b) corresponds to satisfactory crystal structure model indicator (R_B = 0.041) and profile factors (R_P = 0.079 and R_{WP} = 0.098). Due to the departure of half of the quinone molecules, single chains are now present at the center of the tunnels with 50% occupancy (Figure 6). Within one tunnel, the single chain can be nearly parallel either to half of the four organic walls or to the second half. This new orientation of the organic moieties now allows both (i) $\pi-\pi$ interactions between quinone molecules and the benzyl units of the dicarboxylate linkers and (ii) hydrogen bonds to the hydrophilic part of the octahedral chain. It is interesting to note that one oxygen in the quinone molecule is now hydrogen bonded to the OH group of the chains of corner-shared octahedra.

Although not central to this article, mention should be made that the X-ray pattern of **MIL-53(Fe)_quinone$_{0.5}$** remains unchanged when the sample is cooled down to room temperature. With this information in mind, the synthesis of our **MIL-53(Fe)_quinone$_{0.5}$** sample was revisited. The **MIL-53(Fe)_quinone$_{0.5}$** can also be prepared by simply mixing a 1:0.5 molar ratio of **MIL-53(Fe)_vac/**quinone at 130 °C for 2 h and then cooling it to room temperature (Figure 3b). Lower annealing temperatures did not yield this phase regardless of the reaction time (1 week being the maximum time tried).

3.3. NMR Spectroscopy. The ^{13}C NMR spectra of **MIL-53(Fe)_quinone$_1$** is shown in Figure 7. Because these materials are paramagnetic, we rely only on the very fast MAS to remove the ^{13}C−^{1}H dipolar couplings.[29,30] The ^{13}C

(29) Ishii, Y.; Wickramasinghe, N. P.; Chimon, S. *J. Am. Chem. Soc.* **2003**, *125*, 3438.
(30) Kervern, G.; Pintacuda, G.; Zhang, Y.; Oldfield, E.; Roukoss, C.; Kuntz, E.; Herdtweck, E.; Basset, J. M.; Cadars, S.; Lesage, A.; Coperet, C.; Emsley, L. *J. Am. Chem. Soc.* **2006**, *128*, 13545.

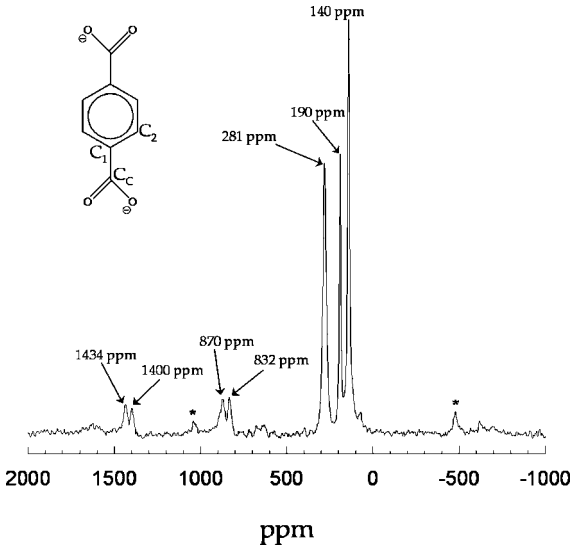

Figure 7. Stacked plot of ^{13}C MAS NMR spectra, acquired at 38 kHz, of **MIL-53(Fe)_quinone$_1$**. The shift of the main isotropic resonances is given, and the spinning sidebands resulting from the MAS are marked by asterisks. A scheme of the benzene dicarboxylate unit that acts as a building block of the structure of MIL-53, with the different non equivalent carbon atoms indicated, is shown.

spectrum of the sample loaded with 1 equivalent of quinone is the simplest to interpret. Two resonances at 140 ppm and 190 ppm are observed and are assigned to the carbonyl and the −CH═CH− groups in the quinone molecules, respectively. Three groups of additional resonances are seen at 281, 870 and 832, 1434, and 1400 ppm. These resonances have shifts outside the typical chemical shift range expected for ^{13}C, and the large shifts are ascribed to the hyperfine or Fermi contact shift, resulting from the transfer of spin density from the Fe^{3+} ions to the *s* orbitals at the different carbon atoms. In general, the fewer the bonds separating the paramagnetic ion from the nucleus under investigation, the larger the hyperfine shift. On this basis, we assign the shifts to 1400/1434, 870/832, and 281 ppm to the carboxylate (C_C), C_1, and C_2 atoms of the BDC framework, respectively (Figure 7). The intensities are in approximate agreement with the relative concentrations of these local environments (1:1:2, for the carboxylate:C_1:C_2). The carboxylate and C_1 resonances are split in two, which is consistent with the structure obtained by high-resolution synchrotron XRD, where two non-equivalent C_1 and C_C are observed per unit cell.

3.4. Electrochemical Behavior. The new **MIL-53(Fe)_quinone$_1$** phase contains two redox centers: the Fe^{3+}/Fe^{2+} redox couple, which has already been reported to charge compensate the reversible exchange of 0.6 Li^+ per Fe in **MIL-53(Fe)**[17] and the quinone molecules, which are electrochemically active toward Li according to the following reaction.[31]

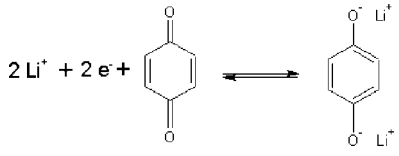

Therefore, on the basis of the existence of both centers and their corresponding capacities, one would expect a

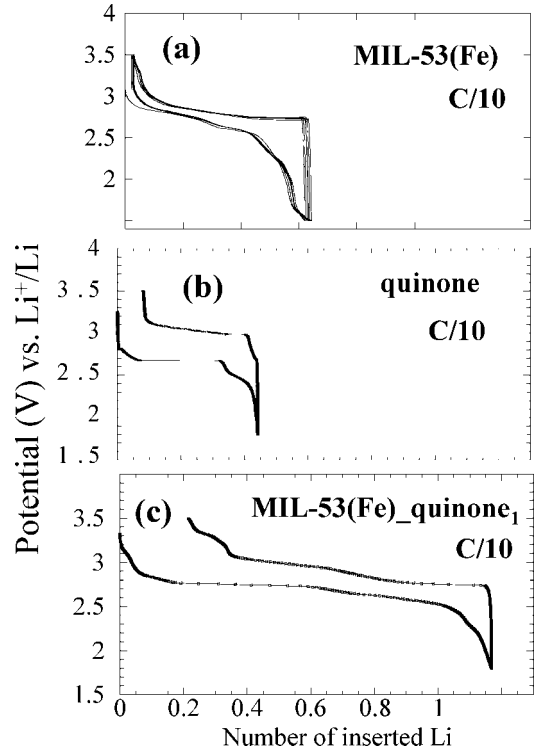

Figure 8. Voltage composition profiles are shown in (a−c) for Li/**MIL-53(Fe)_vac**, Li/quinone, and Li/**MIL-53(Fe)_quinone$_1$** Swagelok cells cycled in the range 1.8−3.5 V at a *C*/10 rate, respectively. Electrodes contained from 5 to 8 mg of active material per cm^2.

cumulative gravimetric capacity of 202 mA h g^{-1} (2.6 exchanged electrons) for the **MIL-53(Fe)_quinone$_1$** phase. Figure 8 shows, for comparison purposes, the potential−composition curve of Swagelok cells using pure quinone (Figure 8a), quinone-free (Figure 8b), and quinone-containing **MIL-53(Fe)** phases (Figure 8c) as the positive electrode. The ability of the quinone-free phase to reversibly accept 0.6 Li^+ per formula unit was confirmed. Unexpectedly, pure quinone was shown to reversibly react only with 0.5 Li, rather than the 2 Li proposed based on the reaction above. This is due to the partial dissolution of quinone molecules into the 1 M $LiPF_6$ EC-DMC electrolytes, as confirmed by complementary IR measurements. Besides this limited capacity, we noted a large polarization (ΔV = 600 mV) indicative of poor electrode kinetics, even though the electrodes were made by mixing carbon and quinone powders in a 50/50 weight ratio. The electrochemical trace for a Li/**MIL-53(Fe)_quinone$_1$** cell is shown in Figure 8c. During the first discharge, the first 0.2 lithium moles (x = 0.2) are inserted through a constantly dropping voltage (indicative of a solid solution process) until the potential reaches a plateau, indicative of a two-phase process, at 2.72 V. This plateau, which extends for 0.4 Li moles and ends at $x = 0.6$, is followed by a smooth drop in potential until $x = 1.05$ and a faster decay until x = 1.2. The overall amount of lithium that can be intercalated into **MIL-53(Fe)_quinone$_1$** equals 1.2, which represents a gravimetric capacity of 93 mA h g^{-1}. The subsequent charge presents three main distinctive features with (i) a plateau, located near 2.72 V, similar to that observed in pure **MIL-**

(31) Pletcher, D.; Thompson, H. *J. Chem. Soc., Faraday Trans.* **1998**, *94*, 3445.

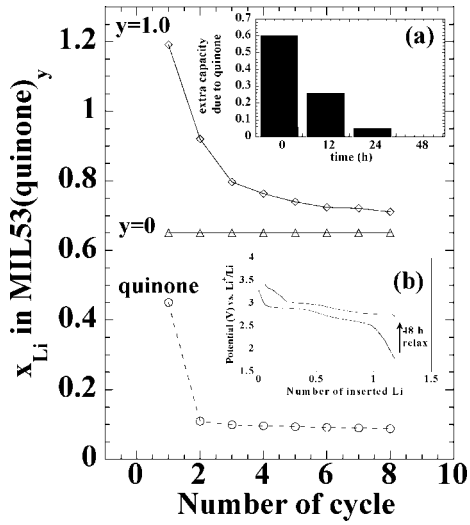

Figure 9. Capacity retentions for three Li/**MIL-53(Fe)_vac**, Li/quinone, and Li/**MIL-53(Fe)_quinone$_1$** Swagelok cells cycled in the range 1.8−3.5 V at a *C*/10 rate are shown together with the variation of the extra cell capacity (inset (a)) associated with the quinone addition as a function of the cell resting time prior to its first discharge, and as a second inset (b) the voltage−composition trace for a Li/**MIL-53(Fe)_quinone$_1$** cell, which rested for 12 h, discharged, and then relaxed for 48 h prior to being recharged.

53(Fe), and accounting for almost 0.4 lithium ions, which is followed by (ii) a sloping voltage domain between $x = 0.7$ and $x = 0.4$, around 3 V, and finally (iii) ends in a high-voltage (near 3.3 V) deintercalation process. The most important difference between quinone-free and quinone-containing electrodes lies in the discharge plateau near 2.7 V seen solely in the latter. Thus, we directly ascribe this plateau to the reduction of the inserted quinone molecules.

An overall benefit of the quinone uptake is an increase in the electrode capacity from 65 mA h g^{-1} to 93 mA h g^{-1}. However, this value is not maintained for too long as the capacity of the **MIL-53(Fe)_quinone$_1$** rapidly decays to reach that of a quinone-free **MIL-53(Fe)** electrode after only five cycles (Figure 9). Such an observation is suggestive of a progressive release upon cycling of the quinone molecules from the **MIL-53(Fe)** host. To test this hypothesis, we checked the effect of resting the battery prior to the cell discharge on its first discharge capacity (Figure 9 inset a). The lowest discharge capacity was observed for the battery left for the longest resting period (48 h), confirming our hypothesis. Thus, an electrolyte-driven leaching of the quinone molecules present in our host **MIL-53(Fe)_quinone$_1$** precursor phase appears to be occurring. When the cell is discharged, the quinone molecules present in the lattice are reduced to quinolate species, which are no longer soluble in the electrolyte. Maintaining the electrode in its discharged state should not therefore affect the electrode capacity. This prediction was experimentally confirmed by the full reversibility displayed by a cell that was discharged, left 24 h on rest, and relaxed 48 h prior to its full recharge (Figure 9 inset b). However, once the recharge is performed, the recovered quinone molecules are again prone to dissolution. Hence, after a few cycles, none of the quinone molecules in the **MIL-53(Fe)** precursor are left to be reduced, leading to the merging of the capacity retention curves after 6−8 cycles. Further insight into the electrochemical reactivity of **MIL-53(Fe)_quinone$_y$** composites has been achieved via in situ XRD measurements and NMR as described next.

In situ X-ray experiments were performed on two separate cells using constant amount of EC-DMC electrolyte (0.2 cm^3) and different amounts of **MIL-53(Fe)_quinone$_1$**, 4 and 20 mg, so as to assess, in addition to the Li-driven structural changes, the propensity for electrolyte−quinone exchange. The electrochemical curve of the cell having the lowest amount of **MIL-53(Fe)_quinone$_1$** does not show any signature of quinone reduction (i.e., no plateau is found at 2.7 V) (Figure 10a). This is consistent with the in situ XRD data, which reveal a phase evolution somewhat similar to that previously observed for a quinone-free **MIL-53(Fe)** sample. The **MIL-53(Fe)_quinone$_1$** structure progressively changes from having a $P2_1/c$ space group [$a = 11.9140(2)$ Å, $b = 6.8775(2)$ Å, $c = 21.3414(3)$ Å, $\beta = 123.67(2)°$ and $V = 1455.33(4)$ Å^3] to an *Imcm* space group [$a = 15.602(3)$ Å, $b = 14.697(2)$ Å, $c = 6.878(1)$ Å, $V = 1577.1(7)$ Å^3] similar to that reported for **MIL-53(Fe)_DMC** phases.[17] In contrast, the cell containing the largest amount of **MIL-53(Fe)_quinone$_1$** shows a plateau at 2.7 V and a higher number of lithium exchanged, the capacity being 2-fold, consistent with the quinone being electrochemically active.

To provide deeper insight into the electrochemical reduction mechanism of an electrode containing quinone, we assembled a third in situ cell with a high amount of active material. The cell was initially left in open circuit for a certain amount of time, during which a rapid evolution of the XRD patterns was observed. As soon as the fresh sample is in contact with the electrolyte extra Bragg peaks corresponding to a **MIL-53(Fe)_DMC**-like structure grow up (see Figure 10b) at the expense of those of **MIL-53(Fe)_quinone$_1$**. This further confirms the rapid quinone/electrolyte solvent exchange, so as to reach an equilibrium which obviously depends on the electrode/electrolyte weight ratio. Once the exchange equilibrium is reached, as deduced from the lack of further changes in the XRD patterns, a current was applied to start the electrochemical process, and a series of patterns was collected as a function of x (Figure 10c). These data were refined using the pattern matching routine of the Fullprof program,[32,33] and the obtained lattice parameters values are plotted in Figure 10d. An initial smooth shift of the lattice parameters was observed, consistent with the corresponding continuous voltage drop in the voltage−composition trace, and linked to the partial reduction of Fe^{3+} to Fe^{2+}. Interestingly, this change in lattice parameter continues during the first half of the 2.72 V plateau, which is generally the signature of a two-phase reaction. Such behavior implies that two redox processes take place in parallel, that is to say, a reduction of bulk "**MIL-53(Fe)_quinone$_c$**", a phase in which the quinone content, *c*, is lower than 1, and of the quinone species that are no longer within the bulk structure, but still connected via adsorption to the surface of the electrode and can therefore be reduced. Such a surface quinone$_{abs}$ → quinolate reduction cannot be detected

(32) Frontera, C.; Rodriguez-Carvajal, J. *Physica B* **2003**, *335*, 219.
(33) Roisnel, T.; Rodriguez-Carvajal, J. EPDIC 7: European Powder Diffraction, Parts 1 and 2;Barcelona, May 20−23, 2000; Scitec Publications: Chennai, India, 2001; Vols. *378−381*, p 118.

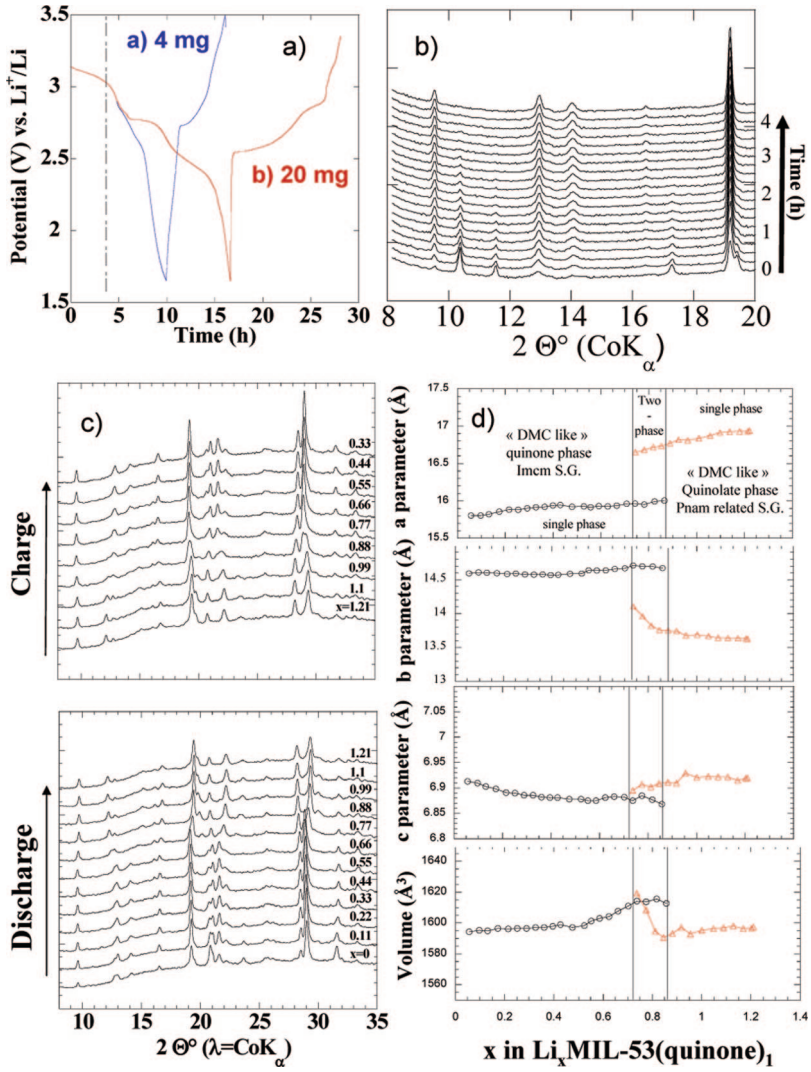

Figure 10. (a) Voltage composition curves for two Li-cells using 4 and 20 mg **MIL-53(Fe)_quinone$_1$** immersed in 0.3 cm^3 of electrolyte. (b) Evolution of the XRD pattern of the **MIL-53(Fe)_quinone$_1$**/Li cell (e.g., containing 20 mg of electrode on rest). An in situ X-ray Li/**MIL-53(Fe)_quinone$_1$** electrochemical cell cycled at *C*/10 between 1.5 and 3.5 V. (c) XRD powder patterns collected during the first discharge (bottom) and charge (top). (d) Evolution of *a*, *b*, *c* lattice parameters and *V* with respect to function of *x*, obtained by refinement from the patterns shown in (c). As the values obtained for the discharge and charge traced each other very closely, consistent with the reversibility of the process, we have solely reported the variation of the lattice parameters for the discharge.

by XRD. Because these two phenomena are in competition and given the presence of core vs surface redox couples that can lead to mixed potentials, further analysis of the potential−composition curve in relation to the structural transformations is hindered.

Upon further discharge beyond $x = 0.7$, a second phase with the same space-group of that of **MIL-53(Fe)_quinone$_1$**, appears at the expense of the "$x = 0.7$" phase. Most likely, the origin of this new phase is related to the reduction of the remaining quinone within the **MIL-53(Fe)** host into quinolate. When the lithium content is greater than 0.85, the voltage evolution is similar to that previously reported for a battery with quinone-free **MIL-53(Fe)**,[15] and only one phase is present (S.G.: *Pnam*, $a = 16.6(1)$ Å, $b = 14.0(1)$ Å, $c = 6.9(1)$ Å, $V = 1604$ Å^3), which suggests further reduction of Fe^{3+} to Fe^{2+} within the **MIL-53(Fe)-quinolate** phase. Upon subsequent charge, the aforementioned processes are reversible, the oxidation of quinolate to quinone species occurring at a higher voltage, thus providing additional time to exchange with the electrolyte. This is considered to be the reason why the quinone is progressively removed from the pores upon cycling, leading to the loss of the corresponding extra capacity.

The ^{13}C NMR spectra of **MIL-53(Fe)_quinone$_1$** samples with different levels of lithium intercalation are shown in Figure 11a. The enlargement of the low frequency region clearly shows that the resonances due to the quinone molecules in the channels (at 190 and 140 ppm), present in the pristine sample, have completely disappeared in the $x_{Li} = 0.45$ sample (Figure 11b). Instead, two new peaks, associated with the alkyl and carbonate groups of either DMC or EC, at 66 and 159 ppm, respectively, are prominent. Because the acquisition delays (0.2 s) used to acquire this data are much shorter than the long relaxation delays (a few seconds) found for typical ^{13}C liquid samples, these resonances likely result from the solvent molecules from the electrolyte (EC/DMC) present in the **MIL-53(Fe)** channels. The Fe^{3+} ions in the **MIL-53(Fe)** chains act as strong relaxation agents (presumably via a dipolar-driven mechanism, because there are no covalent

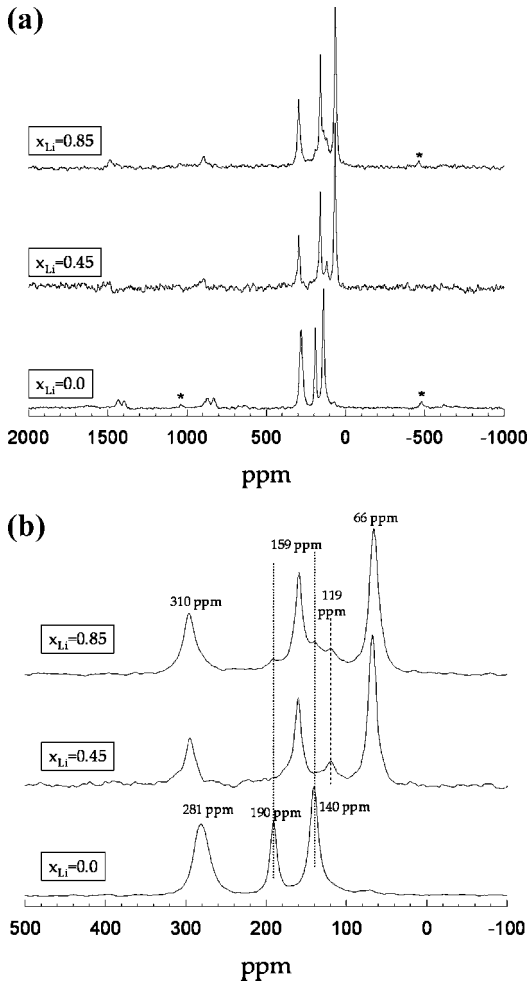

Figure 11. (a) Stacked plot of the ^{13}C MAS NMR spectra, acquired at 38 kHz, of pristine **MIL-53(Fe)_quinone$_1$** and samples resulting from the electrochemical intercalation of the amount of lithium indicated; (b) zoom-in plot of the region from −100 to 500 ppm. The shift of the main isotropic resonances is given, and the spinning sidebands resulting from MAS are marked by asterisks, in this and the subsequent two figures. The dotted and dashed lines indicate the resonances generated by the presence of quinone and quinolate molecules, respectively.

bonds between the host and the guest molecules), thereby reducing the spin−lattice relaxation times of the sorbed molecules. Therefore, the signals corresponding to the quinone molecules are not observed because they are no longer in the channels, in agreement with the in situ XRD results.

Significant changes are also observed for the resonances arising from the **MIL-53(Fe)** framework. The C_2 resonance shifts from 281 to 310 ppm. This is ascribed to the intercalation of EC/DMC into the structure and loss of the quinone molecules, and is consistent with spectra acquired following the addition of DMC directly to a sample of **MIL-53(Fe)_quinone$_1$**. Although much of the DMC evaporated while packing the sample in the glovebox, a shoulder at 310 ppm, ascribed to DMC in the MIL-53 pores, was still observed along with the resonance at 281 ppm. Interestingly, the shift of the C_2 resonance from 266 (dehydrated), 281 (quinone), to 310 ppm appears to correlate with the volume of the **MIL-53(Fe)** pores. The same is true for the C_1 and C_c resonances, which also shift to higher frequencies (Figure 11a). However, a noticeable loss of intensity occurs, suggesting that not all the signals due to these carbon atoms can be observed.

Most relevant to the electrochemical process, a ^{13}C resonance is clearly observed at 119 ppm (Figure 11b) for $x_{Li} = 0.45$, which is assigned to the aromatic carbon atoms in the quinolate. The second weaker resonance of this molecule, due to the alkoxide groups(>C−O$^-$), should resonate at approximately 150 ppm, but is likely masked by the DMC/EC peaks. This confirms that the plateau at 2.72 V is, among other processes, associated with the reduction of the guest molecules. Furthermore, because these quinolate molecules are observed, they must be located inside the **MIL-53(Fe)** channels, suggesting that the reduction process involves small concentrations of quinone molecules either still present in the pores, or more likely, at the entrances to the pores, on the surface of the **MIL-53(Fe)** particles. Once reduced, the quinolate molecules displace the DMC (and EC) molecules and enter the **MIL-53(Fe)** pores, providing additional empty sites for the quinone molecules at the entrances to the pores. This mechanism would account for the difference in reduction potential for the reduction of quinone and the quinone in the **MIL-53(Fe)** composite. On reduction to 1.8 V ($x_{Li} = 0.85$), the intensity of the quinolate resonance remains essentially unchanged, indicating that there is no further reduction of the molecule in this potential window. The low-frequency region is still, however, dominated by the electrolyte solvent molecules. A few weak resonances due to quinone reappear at (at 190 and 140 ppm). This is ascribed to the presence of some quinone molecules that come out of the electrolyte solution when drying the electrolyte. Most likely, these molecules are nearby some Fe^{3+} framework sites that have not been reduced, or on the surface. It is difficult to make any more detailed comparisons because the two samples came from different batteries from different **MIL-53(Fe)_quinone$_1$** batches.

^7Li MAS NMR was performed in order to obtain additional information concerning the structural changes that take place upon insertion of lithium in this composite material. The resulting spectra, shown in Figure 12a, are dominated by a resonance at 0 ppm due to lithium ions in diamagnetic environments, hence with no direct interaction with the iron centers. The diamagnetic environments include Li^+ associated with either PF_6^- (in the electrolyte) or the quinolate. No additional signals were observed for the sample with $x_{Li} = 0.45$, indicating that the additional 0.45 lithium ions interact only with the quinolate ions and are far away from the Fe^{3+} ions. This provides reinforced evidence that the quinone molecules are the redox centers at these voltages. When the compound is further reduced and the lithium content is increased to 0.85, a very small shoulder appears at 17 ppm (see inset in Figure 12a). The range of ^7Li NMR chemical shifts for diamagnetic compounds is known to be very small and does not exceed ± 5 ppm.[34] Consequently, even if small, this shift is consistent with a lithium hyperfine interaction involving the Fe^{3+}/Fe^{2+} ions of the **MIL-53(Fe)**

(34) MacKenzie K. J. D., Smith M. E., *Multinuclear Solid-State Nuclear Magnetic Resonance of Inorganic Materials*; Pergamon Materials Series; Pergamon: Amsterdam, 2002.

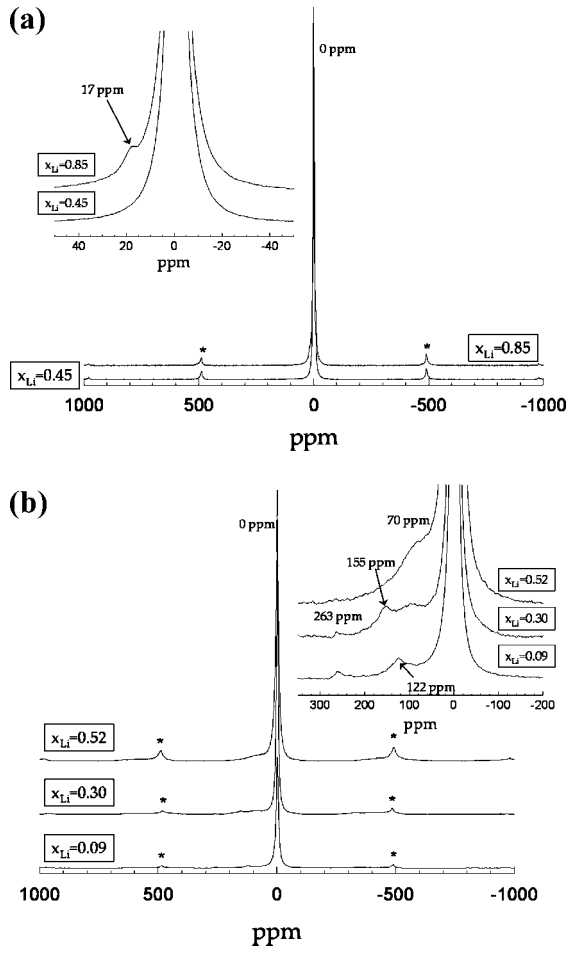

Figure 12. Stacked plot of the ^{7}Li MAS NMR spectra, acquired at 38 kHz, of (a) **MIL-53(Fe)_quinone$_1$** and (b) **MIL-53(Fe)_quinone$_0$** reduced in a lithium battery. The amount of intercalated lithium is indicated. The inset in (a) shows a close-up of the region from 50 to −50 ppm, in which a shoulder at 17 ppm is resolved. The inset in (b) shows a close-up of the region from 350 to −200 ppm.

framework. The small shift is likely due to weak interactions between the Li^+ and the anions (X^{n-}) of the **MIL-53(Fe)** framework, and the small number of Li−X−Fe interactions. This result confirms that the capacity resulting from the process below 2.7 V is due to the reduction of the Fe^{3+} ions in the **MIL-53(Fe)** structure. Exchange processes, between the Li^+ associated with the quinolate and with the **MIL-53(Fe)** framework, may also occur because both Li^+ environments are present inside the **MIL-53(Fe)** pores.

To determine the size of the Li−Fe hyperfine interactions in the absence of the quinone molecules, we performed similar experiments on **MIL-53(quinone)$_0$** (Figure 12b). Now, resonances with noticeable hyperfine shifts are observed even at low lithium contents, consistent with the fact that Fe^{3+} reduction occurs even at these voltages. The hyperfine shifts decrease in magnitude as Fe^{3+} is reduced to Fe^{2+} (e.g., $x_{Li} = 0.09$ vs $x_{Li} = 0.52$). However, even at the maximum insertion level, a large hyperfine interaction of 70 ppm is still observed. This is noticeably larger than the shift observed for **MIL-53(Fe)_quinone$_1$**, (17 ppm), indicating the existence of either stronger and/or multiple Li−X−Fe interactions (per Li^+ ion).

4. Conclusion

The concept of enhancing the electrochemical capacity of **MIL-53(Fe)**, by introducing a guest organic electroactive molecule such as 1,4-benzoquinone within its framework, has been proven. Unfortunately, the extra capacity associated with this guest rapidly fades upon cycling. We demonstrated that this poor capacity retention is due to the progressive exchange between quinone and DMC molecules when the **MIL-53(Fe)** electrode was placed in contact with the electrolyte. Because of the richness of organic chemistry, new sets of electrochemically active guest molecules/MOF are available; therefore, such a research path could greatly benefit from theoretical calculations aimed toward establishing the ranking stability of these new formulations with respect to classical electrolytes. The electrochemical performances of these quinone-loaded materials turn out to be somewhat disappointing. This is in contrast to their fascinating structural chemistry, namely the onset of a temperature-driven phase transition associated to the reordering of the quinone molecules within the MOF channels so as to optimize the $\pi-\pi$ interactions between the benzene rings of both the quinones and the MOFs ligands. Needless to say, a great amount of work regarding the energy of such transformations and more specifically of the interaction between the MIL ligand and the guest molecules remains to be done so as to optimize the design of new phases that could have an impact within the fields of both Li and hydrogen storage.

Acknowledgment. This work was supported by the CNRS and French ANR "CONDMOFs" funding. We want to thank C. Masquelier for the thermal diffraction experiments and Matthieu Courty for the TG and DSC study. C.P.G. and J.C. acknowledge support from the NSF via grant DMR050612 and from the Assistant Secretary for Energy Efficiency and Renewable Energy, Office of FreedomCAR and Vehicle Technologies of the U.S. Department of Energy under Contract DE-AC03-76SF00098, via Subcontract 6517749, with the Lawrence Berkeley National Laboratory. J.C. is indebted to the Generalitat de Catalunya for providing funding through a Beatriu de Pinós postdoctoral fellowship.

CM8032324